Catalysis Science & Technology

Accepted Manuscript

ROYAL SOCIETY OF CHEMISTRY

www.rsc.org/catalysis

Journal Name

MINIREVIEW

Microporous Crystalline Mo-V Mixed Oxides for Selective Oxidations

Satoshi Ishikawa[a, b], Wataru Ueda[a, c]

Received 00th January 20xx,
Accepted 00th January 20xx

DOI: 10.1039/x0xx00000x

www.rsc.org/

Recent developments of crystalline Mo_3VO_x catalysts (MoVO), new type of oxidation catalysts for selective oxidations of ethane to ethene and of acrolein to acrylic acid, are reviewed. MoVO are formed by the building unit assembly of polyoxomolybdates under a hydrothermal condition. These catalysts are comprised of a network arrangement based on $\{Mo_6O_{21}\}^{6-}$ pentagonal unit and $\{MO_6\}$ (M = Mo, V) octahedral to form a hexagonal channel and a heptagonal channel. Among these channels, the heptagonal channel acts as a micropore with 0.40 nm in diameter which can adsorb small molecules such as CO_2, N_2, methane, ethane, etc. The size of the heptagonal channel micropore is reversibly and continuously tunable by redox treatment. Interestingly, the heptagonal channel activates ethane inside and acrolein on the channel located over the external surface. A tuning of the heptagonal channel size significantly modifies the catalytic performance for the selective oxidation of ethane. Strong relationships among crystal structure, microporosity, and catalytic performance were observed. here.

1. Introduction

1.1. Selective oxidation of light alkanes

Transformation of light alkanes into olefin and valuable oxygenated compounds by catalytic selective oxidations has been attracting much attention since this reaction produces important industrial organic chemicals and intermediates, such as alcohols, aldehydes, ketones, acids, and their anhydrides. Recently, an interest for the catalytic selective oxidations is expanding because of shale gas revolution in USA. Therefore, a utilization of light alkanes as a cheap and an abundant feedstock for the catalytic selective oxidations have been attracting further attention. However, in spite of tremendous efforts, only the limited number of processes for selective oxidations of light alkanes are industrialized due to the difficulty to obtain a particular product [1-3].

The difficulty of obtaining desired products by the selective oxidation of light alkanes is largely derived from the chemical property of alkanes, such as (i) no lone pairs of electrons, (ii) no empty orbital, and (iii) little polarity of the C-H bonds [1-5]. For these reasons, light alkanes are poorly reactive, thus severe reaction conditions to activate light alkanes are required. This situation makes it difficult to achieve high selectivity toward the desired products because of many undesirable side-reactions and unavoidable further oxidations of the desired products [4-5]. In order to overcome these problem, Grasselli *et al* introduced important principle, which is now recognized as site-isolation concept [6-8]. This concept points out that active sites must be spatially isolated from each other in order to prevent overoxidation and that the active sites must be comprised of the proper number of hydrocarbon activating elements and proper number of lattice oxygens available for directing the reaction toward the desired products. This idea emphasizes an importance of crystal structure of catalysts, more specifically, a rational design of catalyst structure. After the proposal of this idea, an importance of catalyst synthesis to construct a well-organized crystal structure has been widely recognized in the study area of the catalytic selective oxidation of light alkanes [9-15].

1. 2. Crystalline Mo-V based catalysts

One of the most promising catalyst for the selective oxidation of light alkanes is Mo-V-Te-Nb oxide catalyst (MoVTeNbO) discovered by Mitubishi Chemicals [16-19]. This catalyst showed extremely high catalytic activity for selective (amm)oxidation of propane to acrylonitrile or to acrylic acid and selective oxidation of ethane to ethene [16-21]. Especially, for the ammoxidation of propane, this catalyst has already been commercialized by PTT Asahi Chemical Company Limited with the productivity of acrylonitrile about 200,000 t /y.

There are two main crystalline phases in the active and selective MoVTeNbO catalyst: (i) an orthormhombic structure (space group: Pba2) with a composition of $(Te_2O)_2M_{40}O_{112}$ (M = Mo, V, Nb), called as M1 phase and (ii) a pseudohexagonal structure (space group: Pmm2) with a composition of $(TeO)M_3O_9$ (M = Mo, V, Nb), called as M2 phase. For these phases, M1 phase contains all of the elements needed to complete every elementary steps for the selective (amm)oxidation of propane to acrylonitrile or to acrylic acid, and actually, only the M1 phase MoVTeNbO itself can show a quite high catalytic activity for this reaction [8, 22-23]. M2 phase is reported as a co-catalyst to complete the reaction by helping the sequential

[a] Catalysis Research Center, Hokkaido University, N-21, W-10, Sapporo 001-0021, Japan.
[b] Research Fellow of Japan Society for the Promotion of Science.
[c] Department of Material and Life Chemistry, Faculty of Engineering, Kanagawa University, 3-27, Rokkakubashi, Kanagawa-ku, Yokohama, 221-8686, Japan.
[d] E-mail: uedaw@kanagawa-u.ac.jp; Tel: +81 45 481 5661

Table 1. Development of Mo-V based materials

Year	Development	References
~1995	Discovery of MoVTeNbO	[16-19]
1998~	Application of hydrothermal method to produce Mo-V based materials	[29-30, 33]
2000	Discovery of MoVTeO and MoVSbO with M1 structure	[30]
2000~	Role of crystal plane for selective oxidations	[28], [30]
2003~	Identification of crystal structure of MoVTeNbO	[25-27]
2003	Discovery of Orth-MoVO	[31-32]
2003~	Identification of the constituent elements of Mo-V based materials for selective oxidations	[34-39]
2008~	Electron microscopy	[24, 40-43]
2009~	Computational calculation	[22, 44-46]
2009~	Investigation of the crystal formation mechanism of Mo-V based materials	[47-51]
2012~	In-situ XPS analysis of Mo-V based materials during selective oxidations	[52-53]
2014~	In-situ measurement of electron conductivity during selective oxidations	[54-56]
2014~	Incorporation of additional elements	[57-58]
2014~	Role of micropore of Orth-MoVO for selective oxidations	[59-60]
2015~	Discovery of a relationship between crystal structure around the micropore to the catalytic activity for the selective oxidation of ethane	[61]

oxidation of propylene, formed from propane, to acrylonitrile [23-24]. Accordingly, M1 phase is far more important than M2 phase in the sense of the catalytic oxidation. Basic crystal structure of M1 phase MoVTeNbO is the same with Orth-MoVO in Figure 1 (as shown later). M1 phase MoVTeNbO is comprised of the network arrangement of pentagonal {(Nb)Mo_5} unit with MO_6 (M = Mo, V) octahedral. Due to the arrangement of these units, a hexagonal channel and a heptagonal channel are formed in its *a*-*b* plane which is stacks for each other along with *c*-direction, resulting in the formation of rod-shaped crystal [25]. The center of the {(Nb)Mo_5} pentagonal unit is occupied by Nb and is surrounded by five Mo octahedral. MO_6 (M = Mo, V) octahedral connects two pentagonal units as a linker. Te is located preferentially in the hexagonal channel and partly in the heptagonal channel [25-26]. The detailed elemental composition of this phase determined by ICP, XANES and Rietveld refinement was $Mo_{0.55}^{5+}Mo_{6.76}^{6+}V_{1.52}^{4+}V_{0.17}^{5+}Te_{0.69}^{4+}Nb_{1.0}^{5+}O_x^{2-}$ ($28.34 < x < 28.69$) [27]. For the catalytic reactions, the *a*-*b* plane is responsible to the catalysis. Actually, grind treatment to expose cross-section of the rod, where *a*-*b* plane consists of, significantly enhanced the catalytic performance [28]. It is suggested for MoVTeNbO that the combination of various elements having a different role for the catalysis (ex. Hydrogen abstraction, oxygen insertion, product desorption) makes it possible to complete all the elementary steps smoothly which resulting in the high selectivity toward the desired product. The important point is that each constituting elements is spatially located nearby for each other which allows reaction intermediate to interact the element needed for the next reaction step. The quite high catalytic activity of MoVTeNbO is now recognized due to the proper structural arrangement of the proper elements which are active for each elementary step in the selective (amm)oxidation of propane.

There are several examples of the crystalline Mo-V based catalysts besides MoVTeNbO. From late 1990s, our group has been developing the synthesis of Mo-V based materials by a hydrothermal method and successfully obtained several Mo-V based catalysts with a pure manner [29-30]. In the early stage of the research, we could successfully obtain ternary Mo-V-Te oxide (MoVTeO) and Mo-V-Sb oxide (MoVSbO) with M1 structure by a hydrothermal method [30]. For these materials, Te and Sb were located mainly at the hexagonal channel and partly at the heptagonal channel and structural framework of these was comprised only of Mo and V. This fact suggested us that the binary Mo-V oxide should be obtainable since only Mo and V can constitute the structural framework of M1 structure. By the careful control of the synthesis temperature, synthesis time, precursor, volume, and metals concentration, we could successfully obtain crystalline Mo_3VO_x mixed oxide with M1 structure (Orth-MoVO) for the first time in 2003 [31-32] (Figure 1).

Table 1 summarizes how the Mo-V based oxides with M1 structure were developed during two decades. In early 1990s, Mitubishi Chemicals firstly discovered MoVTeNbO catalyst and demonstrated that this catalyst is active for the selective (amm)oxidation of propane [16-19]. This catalyst had been synthesized by slurry method, in which a mixed solution of stoichiometric Mo, V, Te, and Nb sources are mixed and evaporated, followed by the heat-treatment around 600 °C under an inert gas atmosphere. This synthesis method is simple and a large amount of

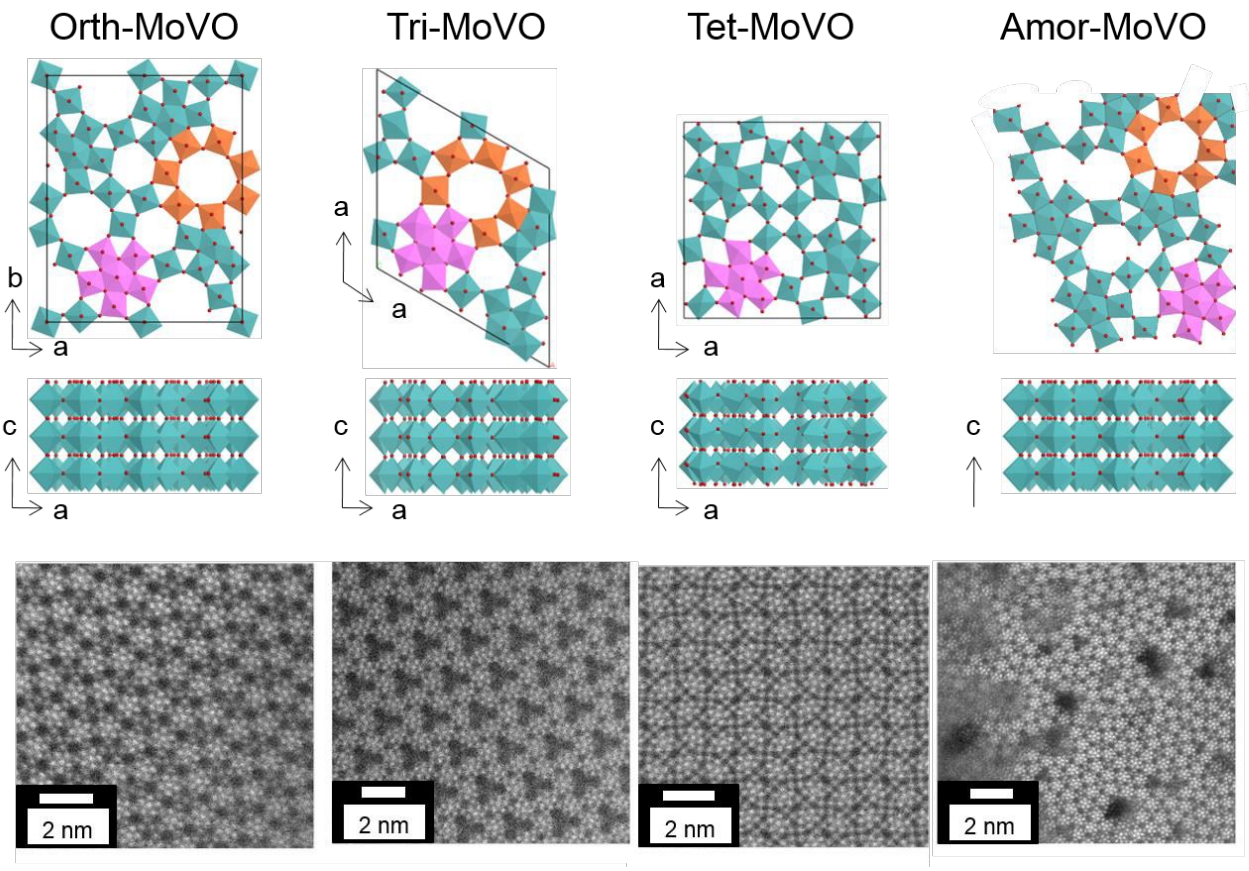

Figure 1. Structural images and HAADF-STEM images of orthorhombic, trigonal, tetragonal, and amorphous Mo_3VO_x. Pink, pentagonal $\{Mo_6O_{21}\}^{6-}$ unit; orange, heptagonal channel. For HAADF-STEM images, white spot represents an element and black spot represents a void space.

the catalyst can be easily obtained. However, the reproducibility was poor and impurities were easily formed simultaneously which caused undesirable catalytic reactions. Thus, the efforts to obtain the pure MoVTeNbO catalyst with M1 phase had been devoted. In late 1990s, since we thought that the formation of Mo-V based mixed oxides was a result of a self-organization of polyoxometalates, we applied a soft synthesis method, hydrothermal method, for the synthesis of Mo-V based materials which was less common method for the synthesis of mixed oxides at that time. As a consequence, we could successfully obtain various Mo-V based mixed materials with a pure manner [29-30]. By applying this method, synthesis of pure M1 MoVTeNbO could be achieved and high reproducibility of this synthesis has been confirmed [20, 33]. After the discovery of the synthesis method of the pure M1 MoVTeNbO, the role of constituent elements for catalytic reactions was revealed [34-39]. In addition, the computer calculation and the electron microscopy have been developed by using the highly pure and crystalline M1 MoVTeNbO as the model [22, 24, 40-46]. Crystal formation mechanism has also attracted much attention since the understanding of this formation mechanism may lead a development of synthesizing an active catalyst [47-51]. In our view point, the recent research topics in these materials are (i) in-situ XPS analysis of Mo-V based materials during selective oxidations [52-53], (ii) In-situ measurement of electron conductivity during selective oxidations [54-56] as that Schlögl *et al* is focusing on, and (iii) incorporation of additional elements to enhance the catalytic activity [57-58].

For the synthesis of Mo-V based materials, we could obtain Orth-MoVO, MoVTeO, MoVSbO, MoVSbNbO with M1 phase. For a development of the oxidation catalyst, an understanding of a structure-activity relationship has been strongly desired. Therefore, we focused on a ternary MoVO system as a simple system. By using this simple MoVO system, we found that a micropore in the MoVO structure worked to activate ethane and acrolein, and recently, the relationship between the structure around the micropore and the catalytic performance for the selective oxidation of ethane. The obtained results provided the molecular level understanding on the catalytic selective oxidation.

1. 3. Crystalline Mo_3VO_x catalysts

We have successfully synthesized Orth-MoVO with M1 structure for the first time by a hydrothermal synthesis. Orth-MoVO is a layered structure. An *a-b* plane forms a slab which stacks for each other to form a rod-shaped material. The *a-b* plane of Orth-MoVO is constructed by a network arrangement based on the pentagonal $\{Mo_6O_{21}\}^{6-}$ unit and the $\{MO_6\}$ (M = Mo, V) octahedra and forms an empty hexagonal and an empty heptagonal channel. The structural model and the HAADF-STEM image of Orth-MoVO are shown in Figure 1.

Orth-MoVO is produced by the hydrothermal synthesis. Interestingly, the control of the precursor solution for the hydrothermal synthesis produced various crystal analogous of Orth-MoVO. For example, a trigonal Mo_3VO_x material (Tri-MoVO) was obtained when the pH of the precursor solution was decreased [62]. An amorphous Mo_3VO_x material (Amor-MoVO), which has an ordered structure for *c*-direction and has a disordered structure for *a-b* plane, was obtained by increasing the concentration of the precursor solution [63]. Apart from the hydrothermal synthesis, it was found that a proper heat-treatment of Orth-MoVO produced a tetragonal Mo_3VO_x material (Tet-MoVO) [63]. These are all the rod-shaped crystal with the elemental composition of Mo_3VO_x (x = 11.2) and are comprised of the same structural parts, pentagonal $\{Mo_6O_{21}\}^{6-}$ unit and MO_6 (M = Mo, V) octahedral. We, therefore, describe these catalysts as 'crystalline Mo_3VO_x catalysts'. Difference of these materials is only the structural arrangement of pentagonal $\{Mo_6O_{21}\}^{6-}$ unit and MO_6 (M = Mo, V) octahedral into the slab where *a-b* plane consists of. Depending on the structural arrangement, Orth-MoVO, Tri-MoVO, and Amor-MoVO form the pentagonal, the hexagonal, and the heptagonal channel in their crystal structure, while Tet-MoVO forms the pentagonal channel and the hexagonal channel. Structure dependency of the catalytic activity will be discussed in chapter 3.

Orth-MoVO showed interesting features derived from an empty heptagonal channel. First, we found that the empty heptagonal channel of Orth-MoVO can work as a micropore with 0.40 nm in diameter which adsorb small molecules like light alkanes [64-66]. This microporous property was, surprisingly, controlled by tuning the reduced state of Orth-MoVO [65-66]. This is the first example that the sorption behavior of an ordered porous crystalline material is continually and reversibly controlled by tuning the reduced state of the materials. Second, Orth-MoVO was found to show an outstanding catalytic activity for the selective oxidation of ethane [63]. Because of the fact that the catalytic activity of Orth-MoVO was far superior to MoVTeNbO, an involvement of the empty heptagonal channel for the reaction has been implied for the selective oxidation of ethane [63, 66]. In addition, Orth-MoVO showed extremely high catalytic activity for the selective oxidation of acrolein to acrylic acid and was superior to industrial catalysts [67-68]. In this case also, the catalytic activity of Orth-MoVO for the selective oxidation of acrolein was far superior to MoVTeO and MoVTeNbO [69]. Therefore, the participation of the empty heptagonal channel for the catalysis has been suggested. The role of the empty heptagonal channel for the catalytic reactions will be discussed in chapter 4 and 5.

The present review provides comprehensive information including crystal formation mechanism (chapter 2) and the structure-activity relationship of the crystalline Mo_3VO_x catalysts (chapter 3 to 5). We believe that the present review provides not only a deep understanding on the catalytic reactions but also an idea to design structurally well-organized catalyst which is active for selective oxidations.

2. Formation mechanism of crystalline Mo_3VO_x catalysts

Orth-MoVO and Tri-MoVO are produced by the hydrothermal reaction of a precursor solution prepared by $(NH_4)_6Mo_7O_{24} \cdot 4H_2O$ (AHM) and $VOSO_4 \cdot nH_2O$. Once the two compounds are mixed in a water, the color of the solution immediately changes to dark-violet by the formation of the giant polyoxomolybdate, $[Mo_{72}V_{30}O_{282}(H_2O)^{56-}(SO_4)_{12}]^{36-}$ ($\{Mo_{72}V_{30}\}$), which consist of 12 pentagonal $\{Mo_6O_{21}\}^{6-}$ polyoxomolybdate units and 30 $[V=O]^{2+}$ units. The formation of $\{Mo_{72}V_{30}\}$ can be confirmed by IR, Raman, and UV as we have shown previously [51]. Since both Orth-MoVO and Tri-MoVO are produced from the precursor solution containing $\{Mo_{72}V_{30}\}$, we assumed that Orth-MoVO and Tri-MoVO are formed by an assembly of building units provided from $\{Mo_{72}V_{30}\}$ under the hydrothermal condition. Table 2 shows the relationship between the concentration of $\{Mo_{72}V_{30}\}$ in the precursor solution and the crystal phase produced from the solution. The concentration of $\{Mo_{72}V_{30}\}$ was controlled by changing the pH of the precursor solution. When no pH control was done (pH = 3.2), 63% of V in the precursor solution took part in the formation of $\{Mo_{72}V_{30}\}$. The increase of pH caused a slight decrease in the $\{Mo_{72}V_{30}\}$ amount. However, the decrease of pH leaded severe decrease in the amount of $\{Mo_{72}V_{30}\}$ due to the transformation of $\{Mo_{72}V_{30}\}$ into more condensed $\{Mo_{36}O_{112}\}$ ($\{Mo_{36}\}$), as confirmed by Raman. After the hydrothermal synthesis, Orth-MoVO can be obtained when no pH control was taken (Entry 5). The decrease in pH to 2.2 leaded the formation of Tri-MoVO (Entry 3). Further decrease in pH leaded the formation of hexagonal $Mo_{0.87}V_{0.13}O_{2.94}$ which contains no pentagonal $\{Mo_6O_{21}\}^{6-}$ unit in the structure (Entry 1, 2). When the pH of the precursor solution increased, only a tiny amount of solid could be obtained (Entry 6) even though enough amount of $\{Mo_{72}V_{30}\}$ was present in the solution. Further increase of the pH to 4.0 produced no solids (Entry 7). Based on these experimental facts, we have proposed a crystal formation process of Orth-MoVO and Tri-MoVO as shown in Scheme 1 (A) [51]. For the formation of Orth-MoVO, dimer of the pentagonal $\{Mo_6O_{21}\}^{6-}$ unit provided from $\{Mo_{72}V_{30}\}$ assembles together with pentamer unit which consists of five $\{MO_6\}$ (M = Mo, V) octahedra to form Orth-MoVO. For the formation of Tri-MoVO, in a reflection of the low pH condition where Tri-MoVO forms, trimer of the pentagonal $\{Mo_6O_{21}\}^{6-}$ unit which is more condensed unit than the dimer unit used for Orth-MoVO formation takes part in the formation of Tri-MoVO with trimer unit which consists of three $\{MO_6\}$ (M = Mo, V) octahedra. When the pH of the precursor solution increased, possibly, the pentagonal $\{Mo_6O_{21}\}^{6-}$ unit cannot condensate to form the dimer or the trimer, building unit for the formation of Orth-MoVO or Tri-MoVO, which inhibit the formation of these materials.

Recently, we found that the seed of Orth-MoVO and Tri-MoVO can work as a crystallization nucleus for the formation of Orth-MoVO and Tri-MoVO [70]. Addition of Orth-MoVO or Tri-MoVO seed crystals resulted in the formation of Orth-MoVO or Tri-MoVO even when the pH of the precursor solution was 4.0 (Entry 8, 9). Since the yield of the solid decreased when unground seed (long rod-shaped crystal) was used, the crystal formation was found to occur from the cross-section of the rods where the *a-a* or the *a-b* plane consists of (Entry 10). Since no formation of Orth-MoVO or Tri-MoVO occurred without $\{Mo_{72}V_{30}\}$, even though the same Mo and V concentration, we concluded that the building units provided by $\{Mo_{72}V_{30}\}$ assembled on the *a-b* or the *a-a* plane of Orth-MoVO and Tri-MoVO

Table 2. pH and concentration of $\{Mo_{72}V_{30}\}$ in the precursor solution, and products amount and their crystal phases after hydrothermal synthesis with or without the seed at 175 °C for 20 h

Entry	pH[a]	Concentration of $\{Mo_{72}V_{30}\}$[b]	$\{Mo_{72}V_{30}\}$ yield[c]	Seed[d]	Crystal of the obtained solid	Amount of solid
1	1.2	0.0 mM	0 %	- e)	Hex-$Mo_{0.87}V_{0.13}O_{2.94}$[f]	6.7 g
2	1.7	0.4 mM	23 %	- e)	Hex-$Mo_{0.87}V_{0.13}O_{2.94}$[f] + Tri-MoVO	-
3	2.2	0.6 mM	35 %	- e)	Tri-MoVO	5.0 g
4	2.7	1.0 mM	57 %	- e)	Orth-MoVO	-
5	3.2	1.1 mM	63 %	- e)	Orth-MoVO	1.4 g
6	3.4	1.0 mM	57 %	- e)	Orth-MoVO	0.3 g
7	4.0	0.9 mM	51 %	- e)	- g)	0.0 g
8	4.0	0.9 mM	51 %	Orth-MoVO	Orth-MoVO	1.3 g
9	4.0	0.9 mM	51 %	Tri-MoVO	Tri-MoVO	1.7 g
10[h]	4.0	0.9 mM	51 %	Orth-MoVO	Orth-MoVO	0.7 g
11[i]	4.0	0.0 mM	0 %	Orth-MoVO	- g)	0.0 g
12	1.2	0.0 mM	0 %	Orth-MoVO	Hex-$Mo_{0.87}V_{0.13}O_{2.94}$[f]	6.9 g

[a] pH of the reaction mixture was changed from 1.0 to 4.0 by adding 2 M H_2SO_4 or 10 wt% ammonia.
[b] Estimated by UV-Vis.
[c] based on V.
[d] seed amount was 0.3 g.
[e] no seed was added.
[f] JCPDF: 00-048-0766.
[g] no solid was obtained.
[h] unground Orth-MoVO seed was added.
[i] V_2O_5 was used as V source.

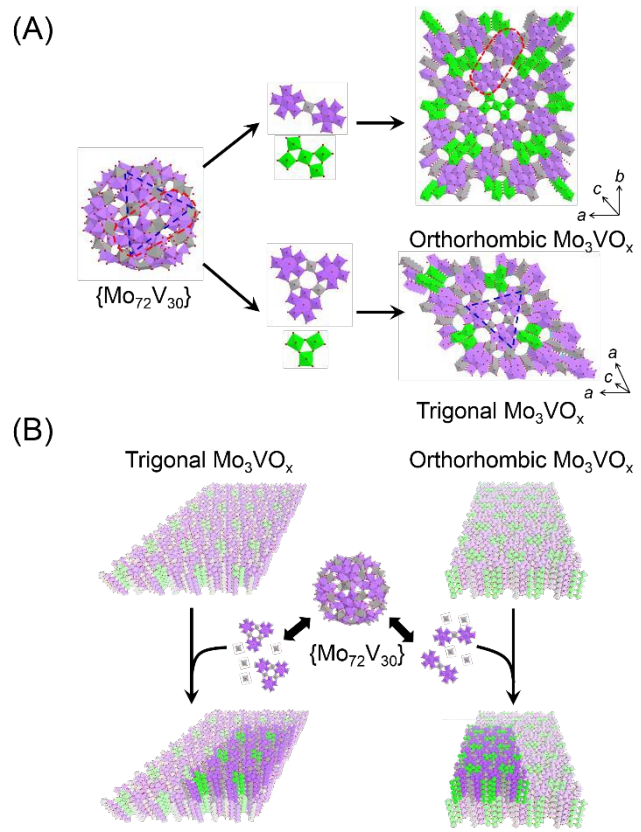

Scheme 1. (A) Proposed schemes of structure formation of orthorhombic Mo_3VO_x and trigonal Mo_3VO_x. (B) Proposed schemes of structure formation in the seed-assisted synthesis. Purple; Mo, gray; V, green; mixture of Mo and V.

to form the rod-shaped crystals (Entry 11, 12). $\{Mo_{72}V_{30}\}$, Orth-MoVO, and Tri-MoVO contain the common structural parts, pentagonal $\{Mo_6O_{21}\}^{6-}$ unit linked with V octahedral, so that the structural parts are thought to preferentially assemble to the *a*-*b* or the *a*-*a* planes of Orth-MoVO or Tri-MoVO. In zeolite synthesis, the hydrothermal synthesis of zeolite in the presence of zeolite seeds has widely been studied [71-75]. In this case, the seed zeolites and the reactant gel need to have the same structural units. When the zeolite seeds and the reactant gel contain the same structural units, the structural units in the gel stack on the surface of the seed crystal, and the zeolite having the same crystal phase with the seed can be formed. Our seed-assisted synthesis of Orth-MoVO and Tri-MoVO seems to be very similar to the seed-assisted synthesis of zeolite. On the basis of these facts, we proposed the crystal formation scheme of Orth-MoVO and Tri-MoVO in the presence of the seed (Scheme 1 (B)) [70]. When the seed is present in the precursor solution, the building units provided from $\{Mo_{72}V_{30}\}$ stack on the cross-section of the seeds to form the rod-shaped material having the same crystal structure with the seed. In this case, $\{Mo_{72}V_{30}\}$ only contributes to the crystal growth for the formation of Orth-MoVO and Tri-MoVO.

On the basis of these experiments, we concluded that Orth-MoVO and Tri-MoVO are produced by the building unit assembly via giant polyoxometalate, $\{Mo_{72}V_{30}\}$ [51, 70]. Building block assembly using giant polyoxometalate will be one of an effective way to create structurally well-organized materials like as Orth-MoVO and Tri-MoVO.

3. Structure-activity relationship for the selective oxidation of ethane and acrolein

Table 3. Relationship between micropore and catalytic activity

Catalyst	Elemental composition[a] (V / Mo)	Number of 7-membered ring /100 nm^2	External surface area[b] /m^2 g^{-1}	Micropore volume[b] /cm^3 g^{-1}	Ethane conv.[c] /%	ACR conv.[d] /%
Orth-MoVO	0.38	73	7.2	14.0	42.2	53.8
Tri-MoVO	0.32	68	18.0	4.0	25.2	99.8
Tet-MoVO	0.38	0	2.7	0	<1	<1
Amor-MoVO	0.38	10~30	5.7	2.8	5.9	9.7

[a] Determined by ICP.
[b] Measured by N_2 adsorption at liquid N_2 temperature and estimated by t-plot method.
[c] Reaction condition: catalyst amount, 0.5 g; reaction gas feed, $C_2H_6/O_2/N_2$ = 5/5/40 ml min^{-1}; reaction temperature, 313 ~ 319 °C.
[d] Reaction condition: catalyst amount, 0.25 g, reaction gas feed, ACR/O_2/H_2O/N_2/He = 2.5/8.0/27.1/39.5/30.5 ml min^{-1}; reaction temperature, 217~218 °C. ACR represents acrolein.

We demonstrated structure-activity relationship using the synthesized crystalline Mo_3VO_x catalysts in the selective oxidation of ethane and acrolein. As we have shown in the introduction, we have successfully obtained 4 distinct crystalline Mo_3VO_x materials (Figure 1); orthorhombic MoVO (Orth-MoVO), trigonal MoVO (Tri-MoVO), tetragonal MoVO (Tet-MoVO), and amorphous MoVO (Amor-MoVO). These materials are all rod-shaped crystal with almost the same elemental composition and are comprised of the structural arrangement based on the pentagonal $\{Mo_6O_{21}\}^{6-}$ unit and $\{MO_6\}$ (M = Mo, V) octahedral, while the arrangement of these units are different for the catalysts. Among the obtained materials, Orth-MoVO, Tri-MoVO, and Amor-MoVO possessed the heptagonal channel (shown as orange in Figure 1) in the structure, while Tet-MoVO had no heptagonal channel. Table 3 shows the numbers of the heptagonal channels in 100 nm^2. The numbers of the heptagonal channels of Orth-MoVO and Tri-MoVO were almost the same and were 73 for Orth-MoVO and 68 for Tri-MoVO. The number of the heptagonal channels of Amor-MoVO was considerably low compared with those of Orth-MoVO and Tri-MoVO (10~30 in 100 nm^2) because of the ununiform structural arrangement as observed in HAADF-STEM image. Table 3 shows the micropore volume of these materials measured by N_2 adsorption. Orth-MoVO, Tri-MoVO, and Amor-MoVO showed microporosity. On the other hand, Tet-MoVO showed no microporosity. Since the difference between Tet-MoVO and other crystalline Mo_3VO_x materials are whether the heptagonal channel is present in the structure or not. Therefore, the heptagonal channel was found to work as a micropore. According to the adsorption experiments using various molecules, the size of the heptagonal channel was determined to be 0.40 nm [61, 64-66]. The micropore volume observed in Orth-MoVO was apparently higher than those of Tri-MoVO and Amor-MoVO (Orth-MoVO, 14.0 cm^3 g^{-1}; Tri-MoVO, 4.0 cm^3 g^{-1}; Amor-MoVO, 2.8 cm^3 g^{-1}). The small micropore volume of Amor-MoVO can be explained due to the low number of the heptagonal channels in the structure. However, Tri-MoVO showed obviously lower micropore volume than that of Orth-MoVO despite of the similar number of the heptagonal channels in 100 nm^2 (Table 3). As we have observed by the HAADF-STEM analysis that Tri-MoVO contained some additional elements inside the heptagonal channel, this situation may decrease the number of the micropores [76-77].

Then, we evaluated the effect of the heptagonal channel for the catalytic reaction. Table 3 shows the substrates conversion for the selective oxidation of ethane and acrolein. For both the reactions, Orth-MoVO, Tri-MoVO, and Amor-MoVO showed catalytic activity, while Tet-MoVO was inactive. These astonishing results indicate that the heptagonal channel is responsible for these catalytic reactions. For the ethane oxidation at 313~319 °C, Orth-MoVO showed higher catalytic activity (42.2%) than those of Tri-MoVO (25.2%) and Amor-MoVO (5.9%). The order of the micropore volume was well matched with the order of the catalytic activity. The participation of the heptagonal inner channel for the oxidation of ethane is implied. On the contrary, Tri-MoVO showed the best catalytic activity for the oxidation of acrolein, followed by Orth-MoVO, Amor-MoVO, and Tet-MoVO (almost inactive). In consideration of the higher external surface area of Tri-MoVO (18.0 m^2 g^{-1}) than that of Orth-MoVO (7.2 m^2 g^{-1}), the order of the catalytic activity for the selective oxidation of acrolein can be described as Tri-MoVO ≅ Orth-MoVO > Amor-MoVO > Tet-MoVO (inactive). This order was well matched with the order of the number of the heptagonal channels in 100 nm^2 (Table 3). This result implied that the heptagonal channel located in the external surface takes part in the catalytic oxidation of acrolein. Although the heptagonal channel is essential for both the reaction, the catalysis field may be different depending on the nature of the substrate.

In this section, we demonstrated the clear structure-catalytic activity relationship for the selective oxidation of ethane and acrolein using the 4 distinct crystalline Mo_3VO_x catalysts. It is obvious that the empty heptagonal channel involves both the reactions. In the next section, we show the role of the heptagonal channel for both the reactions.

4. Role of micropore for the selective oxidation of ethane and acrolein

4. 1. Synthesis of various size of orthorhombic Mo_3VO_x with the same microporosity

In this section, we demonstrate the role of the heptagonal channel for the selective oxidation of ethane and acrolein. In order to understand the role of the heptagonal channel, we synthesized a

Table 4. Rod size, external surface area, and micropore properties of the catalysts

Catalyst	Rod-shaped crystal			Surface area /m^2 g^{-1}			Micropore volume[d] /10^{-3} cm^3 g^{-1}
	Average diameter[a] /μm	Average length[a] /μm	Aspect ratio[b] /-	External surface area[c]	Side area	Section area	
Orth-MoVO	0.40	1.8	4.5	7.2	6.5	0.7	17.7
Orth-MoVO (ng)[e]	0.39	7.9	22.3	6.8	6.6	0.2	22.3
MoVO-$SDS_{0.15}$ (175)	0.44	2.0	4.5	7.2	6.5	0.7	16.6
MoVO-$SDS_{0.30}$ (175)	0.45	1.5	3.3	7.3	6.3	1.0	18.8
MoVO-$SDS_{0.60}$ (175)	0.21	0.7	3.5	14.0	12.1	1.9	17.3
MoVO (230)	0.76	3.7	4.9	5.3	4.8	0.5	16.7
MoVO-$SDS_{0.15}$ (230)	1.04	4.8	4.6	1.2	1.1	0.1	16.6
MoVO-$SDS_{0.30}$ (230)	0.99	3.4	3.4	3.9	3.4	0.5	18.5
MoVO-$SDS_{0.60}$ (230)	0.95	3.5	3.7	5.5	4.8	0.7	16.1

[a] Average of 100 crystallites in SEM images.
[b] Ratio of average length to average diameter of the rod.
[c] Measured by N_2 adsorption at liq. N_2 temperature and determined by *t*-plot method.
[d] Measured by ethane adsorption at room temperature and determined by DA method.
[e] Orth-MoVO without grind treatment.

number of Orth-MoVO catalysts with different external surface areas but with the same micropore volumes by controlling the crystal size. We used anionic surfactant, sodium dodecyl sulphonate (SDS, $C_{12}H_{25}SO_3Na$), to control both a nucleation rate and a crystal growth rate [78-79]. The amount of the addition of SDS was set as SDS / (Mo+V) = x (x = 0, 0.15, 0.30, and 0.60), where x shows the molar ratio between SDS and (Mo+V). The synthesized materials are abbreviated as MoVO-SDS_x. Besides the SDS adding, the temperature in the hydrothermal synthesis was controlled since the hydrothermal temperature affects both a nucleation rate and a crystal growth rate [80-81]. The synthesis temperature y (y = 175 °C or 230 °C) is described at the end of the material name like as MoVO-SDS_x (y). All the synthesized catalysts were ground with a mortar prior to the reaction in order to expose the cross-section of the rod. We also used Orth-MoVO without the grind treatment (Orth-MoVO (ng)). All the synthesized materials showed the XRD patterns attributable to Orth-MoVO and no peaks related to impurities were observed. Elemental composition of these materials determined by ICP-AES was identical. Table 4 summarizes the size of the rod-shaped materials measured by using SEM images and its external surface area and microporosity measured by N_2 or ethane adsorption. All the characterizations were carried out for the catalysts after the selective oxidation of ethane. The crystal size of Orth-MoVO catalysts was clearly changed by the introduction of SDS or by the control of the synthesis temperature due to the change in the nucleation rate and crystal growth rate. The most intense difference in the crystal size could be seen among Orth-MoVO, MoVO-$SDS_{0.60}$ (175), and MoVO-$SDS_{0.15}$ (230) and is shown in Figure 2 (inlet images) and Table 4. It is interesting to note that the aspect ratio, the ratio between the length and the diameter of the rods, was almost the same for the materials, indicating that the shape of the rods was the same regardless of the addition of SDS or of the synthesis temperature. Based on these facts, we successfully obtained Orth-MoVO catalysts with different crystal size and the same crystal shape by adding SDS or by controlling the synthesis temperature.

N_2 adsorption experiment was carried out in order to determine their external surface areas. Depending on the crystal size of the catalysts, the estimated external surface areas were drastically changed (Table 4). On the other hand, the micropore volume of the materials estimated by the ethane adsorption experiment was almost the same in the studied materials and was in the range of 16.1×10^{-3} ~ 22.3×10^{-3} cm^3 g^{-1} (Table 4). Theoretical micropore volume calculated by assuming that ethane adsorbs in the heptagonal channel was 22.4×10^{-3} cm^3 g^{-1}. The observed micropoe volumes were slightly lower than the theoretically obtained value except Orth-MoVO (ng). The grinding treatment may cause dislocation in the *a-b* plane which decrease the number of micropores being capable of adsorbing ethane. Nevertheless, the ethane adsorption results evidently confirm the existence of the heptagonal channel micropore where ethane molecules can freely access. We concluded that the studied materials were with different external surface area but with the same micropore volume.

4. 2. Crystal size dependency on the catalytic activity

The selective oxidations of ethane to ethene and of acrolein to acrylic acid were carried out by using the Orth-MoVO catalysts with the different external surface area and the same micropore volume. For both the reactions, the participation of the heptagonal channel was evidenced as has been shown in chapter 3. Here, a catalytically active part relating to the heptagonal channel is elucidated by evaluating the dependency of the catalytic activity on the external surface area. Figure 2 shows substrates

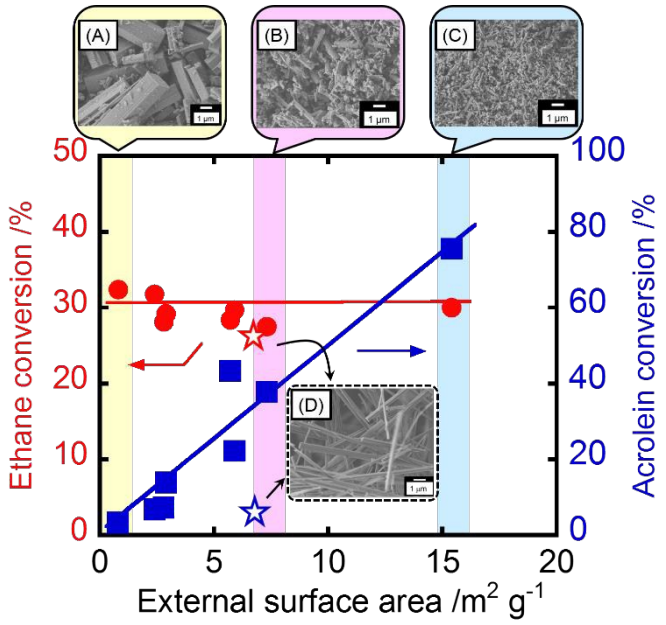

Figure 2. Ethane conversion as a function of external surface area of the catalysts (red circle). Reaction condition of ethane oxidation: catalyst amount, 0.50 g; reaction gas feed, $C_2H_6/O_2/N_2$ = 5/5/40 ml min^{-1}; reaction temperature, 300 °C. Acrolein conversion as a function of external surface area of the catalysts (blue square). Reaction condition of acrolein oxidation: catalyst amount, 0.125 g; reaction gas feed, Acrolein/O_2/H_2O/N_2/He = 2.5/8.0/27.1/39.5/30.5 ml min^{-1}; reaction temperature, 220 °C. Red star and blue star represent the ethane conversion and acrolein conversion of Orth-MoVO (ng), respectively. SEM images of (A) MoVO-$SDS_{0.15}$ (230), (B) Orth-MoVO, (C) MoVO-$SDS_{0.60}$ (175), and (D) Orth-MoVO (ng) after the ethane oxidation are represented.

conversion as the function of the external surface area of Orth-MoVO catalysts. The ethane oxidation was carried out at 300 °C and the acrolein oxidation was carried out at 220 °C. The external surface area was almost maintained even after the reactions. Stars represent the substrates conversion over Orth-MoVO (ng). Obtained products by the ethane oxidation were ethene, COx, and acetic acid. Almost the same selectivity was observed in the studied catalysts and the selectivity to ethene was around 90%. In the case of the acrolein oxidation, obtained products were acrylic acid, COx, and acetic acid. In this case also, product selectivity was almost the same in the studied catalysts and the selectivity to acrylic acid was aroud 95%. For the ethane oxidation, the ethane conversion over the catalysts was ca. 30% and was almost the same regardless of the change of the external surface area (Figure 2, circle). This result indicates that the external surface of Orth-MoVO less contributes to the catalytic activity for the selective oxidation of ethane. It can be concluded that ethane is converted mainly in the micropore channel. Actually, molecular size of ethane (0.40 nm) is almost the same with that of the heptagonal channel micropore (0.40 nm) and it has already been confirmed the fact that the micropore can adsorb ethane (Table 4). In addition, according to Monte Carlo simulation, the highest ethane adsorption energy was obtained when ethane molecule is confined inside the heptagonal channel. Diffusion effects were studied in this catalyst by evaluating the dependency of the catalytic activity on the contact time using MoVO-$SDS_{0.60}$ (175), Orth-MoVO, and MoVO-$SDS_{0.15}$ (230), in which the average crystal size was apparently different for each other. As the result, almost no difference in the dependency of the catalytic activity on the contact time was observed in these catalysts, indicating that Orth-MoVO oxidizes ethane catalytically without diffusion effects. The unground catalyst, Orth-MoVO (ng), showed the comparable catalytic activity with the ground catalyst for this reaction (Figure 2, red star). Since the external surface of Orth-MoVO less contributes to the catalytic reaction, the micropore in the whole particle should involve in the ethane oxidation. Based on the above results and discussions, we concluded that ethane molecule enters the heptagonal channel micropore and goes through without diffusion barrier under the reaction condition. During ethane going through the heptagonal channel, the ethane oxidation takes place and forms ethene inside the heptagonal channel.

On the contrary, the acrolein conversion clearly depended on the external surface area of the catalysts (Figure 2, square). The liner relationship between the acrolein conversion and the external surface area unambiguously indicates that acrolein is converted on the external surface. Since the participation of the heptagonal channel micropore for the selective oxidation of acrolein has been implied by the comparison of 4 distinct crystalline Mo_3VO_x catalysts, it is apparent that the heptagonal channel which is present over the external surface of the catalyst should catalyze acrolein. In this case, the contribution of the side surface of the rods can be easily excluded because of the fact that Orth-MoVO (ng), having almost the same side surface area and far less section surface area compared with Orth-MoVO, showed far less catalytic activity. Based on these experimental facts, we concluded that acrolein is activated over the heptagonal channel present in the external surface of the cross-section of the rod-shaped crystals (*a*-*b* plane). The mouth of the heptagonal channel on the cross-section of the rod might effectively trap the aldehyde group in acrolein and convert to form acrylic acid.

We concluded, on the basis of the above results, that both ethane and acrolein are activated at the heptagonal channel micropore. However, ethane is activated inside the channel and acrolein is activated on the mouth of the heptagonal channel. The catalysis field of the heptagonal cannel was found to be strongly depended on the nature of the substrates.

5. Relationships between crystal structure, microporosity, and catalytic performance

5. 1. Relationship between crystal structure and microporosity

In this chapter, we introduce the relationships between the crystal structure around the heptagonal channel, microporosity, and catalytic activity for the selective oxidation of ethane. Since it was found that the oxidation of ethane takes place inside the heptagonal channel micropore, we thought that the bulk properties in Orth-MoVO should strongly affect the catalytic activity for the selective oxidation of ethane. Orth-MoVO is amenable to the characterizations in a reflection of its high crystallinity. Therefore, the use of this catalyst for the catalytic reaction allow us to understand the structure-activity relationship, unambiguously, and

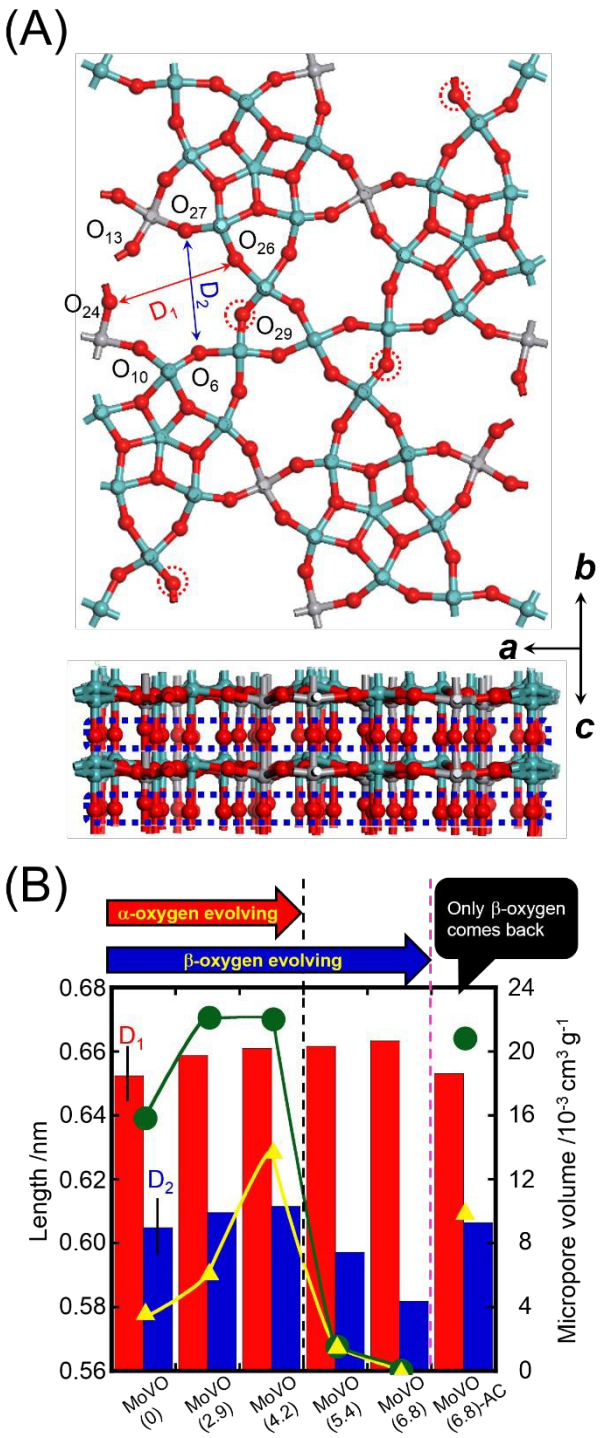

Figure 3. (A) Structural model of Orth-MoVO (Mo, light green; V, gray; O, red). Red circle (top image, O_{29}) is α-oxygen and blue circle (bottom image) is β-oxygen. (B) Left side: diameters of the heptagonal channel. Diameters were determined on the basis of atomic positions of oxygen. Red bar, D_1 (O_{24}-O_{26}, long axis); blue bar, D_2 (O_6-O_{27}, short axis). Right side: micropore volumes of Orth-MoVO with each reduction state measured by C_2H_6 adsorption (green circle) and C_3H_8 adsorption (yellow triangle) and estimated by the Dubinin-Astakhov (DA) method.

enable us to understand the catalytic reaction at molecular level. Such a knowledge is surely fruitful for developing new oxidation catalysts. We have reported that the size of the heptagonal channel is reversibly and continuously controllable by a redox treatment. Since ethane is converted to ethene in the heptagonal channel, the tuning of the heptagonal channel size should affect the catalytic activity. Based on this perspective, we prepared Orth-MoVO with various reduced state by reduction treatment.

First, Orth-MoVO was calcined at 400 °C for 2 h and then, the calcined Orth-MoVO was reduced under 5% H_2/Ar flow at 400 °C with varying the temperature holding time. The catalysts obtained were abbreviated as MoVO (δ), where δ is the amount of the lattice oxygen evolved from the unit cell (represented as $Mo_{29}V_{11}O_{112-\delta}$) by the reduction and was measured by TPR and TG. MoVO (0) means the Orth-MoVO after the air calcination at 400 °C for 2 h. The catalyst oxidized at 400 °C for 2 h under air atmosphere after the reduction treatment was abbreviated as MoVO (δ)-AC. All the catalysts showed the XRD pattern attributable to Orth-MoVO and no impurities were observed by XRD regardless of the redox treatment. No morphological changes were observed by SEM. These results indicate that the Orth-MoVO is stable under the redox treatments and oxidation-reduction of the solid proceeds uniformly.

Figure 3 shows the structural model of Orth-MoVO (A) and the heptagonal channel size change and the microporosity change by the redox treatment (B). Orth-MoVO had two types of the lattice oxygen in the unit cell. One is the oxygen evolved by the early stage in the reduction and hardly comes back to the structure by the re-oxidation. The other is the oxygen evolved continuously with the reduction and reversibly comes back to the structure by the re-oxidation. We abbreviated the former oxygen as 'α-oxygen' and the latter oxygen as 'β-oxygen'. Detailed characterization revealed that α-oxygen is the oxygen in the pentamer unit which faces to the heptagonal channel (O_{29} in Figure 3 (A)) and β-oxygen is the axial oxygen which connects the metals to *c*-axis (blue enclosure in Figure 3 (A)). It was found that the occupancy of α-oxygen rapidly decreased with the reduction and the occupancy reached almost 0 by the reduction up to MoVO (4.2), although β-oxygen can be continuously evolved by the further reduction. In the case of MoVO (6.8)-AC, since α-oxygen can hardly come back to the structure by the re-oxidation, this catalyst contained almost no α-oxygen, although β-oxygen was come back to the structure by the re-oxidation treatment. Figure 3 (B) shows the size of the heptagonal channel for the samples with various reduced states and the micropore volumes measured by ethane or propane adsorption. The size of the heptagonal channel was estimated using the structural model obtained from a single crystal analysis and a Rietveld analysis. The lengths of the heptagonal channel in a long axis (D_1: O_{24}-O_{26}) and a short axis (D_2: O_6-O_{27}) are shown by red bar and blue bar, respectively. For D_1, the length increased with the increase of the reduction degree due to the lattice expansion. For D_2, the length increased by the reduction up to MoVO (4.2). However, the length significantly decreased by the further reduction. By the Rietveld analysis, an expansion of the pentagonal $\{Mo_6O_{21}\}^{6-}$ unit was indicated. Therefore, the decrease in D_2 should be derived from the movement of the atoms in the pentagonal unit toward the heptagonal channel. The adsorption experiments using ethane and propane were carried out for the samples with various

reduced states. Interestingly, the decreases in the micropore volumes were observed by the reduction above MoVO (4.2) (Figure 3 (B)). Since the heptagonal channel works as the micropore to adsorb small molecules, the decrease in D_2 might relate to the diminishment in the microporosity. Re-oxidation of MoVO (6.8) restored D_2, which resulted in the restoration of the microporosity (Figure 3 (B)).

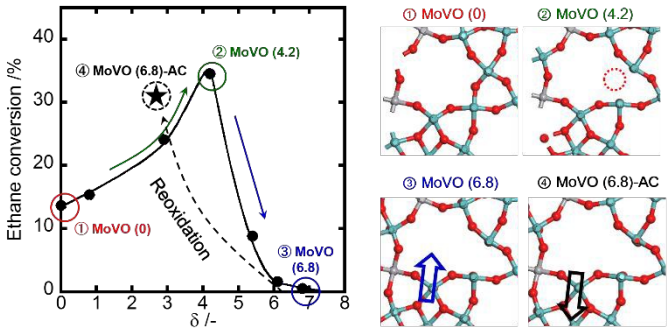

Figure 4. Explanation of the catalytic activity change on the basis of the catalyst structure.

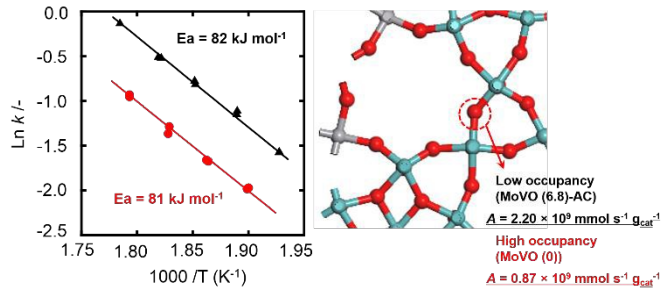

Figure 5. Arrhenius plot for ethane conversion over MoVO (0) (circle) and MoVO (6.8)-AC (triangle). *k* represents the reaction rate constant. Although no change was observed in the activation energy between them, the occupancy of α-oxygen affected frequency factor (*A*) for the selective oxidation of ethane.

Propane adsorption experiment showed interesting profile against the reduction degree (Figure 3, yellow triangle). With the increase of the reduction degree up to MoVO (4.2), the propane adsorption capacity increased. Such the increase could not be seen in the ethane adsorption. Further increase in the reduction degree significantly decreased the propane adsorption capacity in the same manner with the ethane adsorption capacity due to the decrease in the length of the heptagonal channel in short axis (D_2). The molecular size of ethane and propane is 0.40 nm and 0.43 nm, respectively. In consideration with the heptagonal channel size (0.40 nm), ethane can freely access to the heptagonal channel. On the other hand, propane has some difficulty to access to the heptagonal channel. An increase of the heptagonal channel size is essential to adsorb propane. Desorption of α-oxygen is a presumable reason for the increase in the propane adsorption capacity since α-oxygen is facing to the heptagonal channel so that the desorption of α-oxygen can expand the heptagonal channel size. In the same reason, the propane adsorption capacity of MoVO (6.8)-AC was much higher than that of MoVO (0) of which were treated under the same oxidative condition and had almost the same physicochemical properties except the residence of α-oxygen. The partial structural changes including the evolution of α-oxygen and the expansion of the pentagonal $\{Mo_6O_{21}\}^{6-}$ were found to affect the size of the heptagonal channel which resulted in the significant change in their microporosity.

5.2. Relationship between microporosity and catalytic performance

Since Orth-MoVO activates ethane inside the heptagonal channel, the microporosity derived from the heptagonal channel is expected to affect the catalytic activity. Figure 4 shows the ethane conversion of the catalyst as a function of δ. When δ was in the range of 0 ~ 4.2, ethane conversion increased with the increase of δ (from 14% to 33%). However, the ethane conversion dropped drastically when δ was increased to 5.4 (9%) and became almost 0 when δ = 6.8. The ethane conversion of MoVO (6.8)-AC was 31% and was almost the same with that of MoVO (4.2). Selectivity to ethene was decreased in the δ range of 0 ~ δ ~ 4.2 from 88.5% to 76.8% due to the increase of the selectivity to CO_x. Further reduction increased the selectivity to ethene to 93.3%. Ethene selectivity of MoVO (6.8)-AC was 84.4%. In consideration of the physicochemical properties of MoVO (0) and MoVO (6.8)-AC, the major difference is only the occupancy of α-oxygen. Therefore, it is obvious that the occupancy of α-oxygen is the critical factor for the ethane oxidation. This explanation has no conflict for the increase of the catalytic activity in the range of MoVO (0) to MoVO (4.2) because the occupancy of α-oxygen rapidly decreases against δ and reaches to almost 0 when δ reached to 4.2. For the decrease in the catalytic activity by the reduction above MoVO (4.2), we showed that the reduction above MoVO (4.2) caused the expansion of the pentagonal $\{Mo_6O_{21}\}^{6-}$ unit which resulted in the decrease in the microporosity. Since Orth-MoVO activates ethane inside the heptagonal channel, no conversion should occur if ethane cannot go into the channel. Therefore, the decrease in the catalytic activity by the reduction above MoVO (4.2) is derived from the decrease in the length of the heptagonal channel, which prohibit ethane from going through the heptagonal channel. The microporosity changes caused by the partial structural changes around the heptagonal channel were found to strongly affect the catalytic activity for the selective oxidation of ethane.

Then, we discuss how the catalytic activity increased by the decrease of the α-oxygen occupancy. For this purpose, we took Arrhenius plot for MoVO (0) and MoVO (6.8)-AC. The obtained result is shown in Figure 5. No change in the slope of the line was observed between them, and the calculated activation energy was 81 ~ 82 kJ mol^{-1}. Frequency factor, however, was much different and the frequency factor of MoVO (6.8)-AC was 3 times higher than that of MoVO (0) (Frequency factor: MoVO (0), 0.87×10^9 mmol s^{-1} g_{cat}^{-1}; MoVO (6.8)-AC, 2.20×10^9 mmol s^{-1} g_{cat}^{-1}). This result clearly indicates that the increase of the catalytic activity by the evolvement of α-oxygen was due to the increase of the number of the active sites in the structure. In consideration with the structural model of Orth-MoVO, the heptagonal channel with α-oxygen defect should relate to the catalysis field where ethane oxidation can take place.

We propose a reaction scheme of the selective oxidation of ethane with Orth-MoVO (Scheme 2). There are two important points

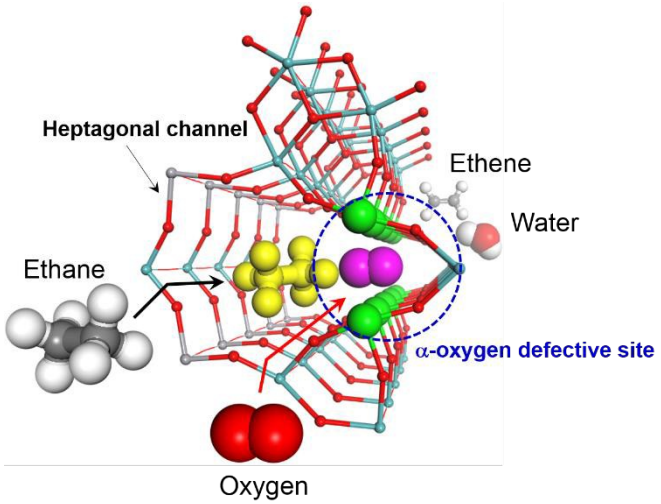

Scheme 2. Conversion of ethane to ethene in the heptagonal channel. Ethane and oxygen marked with yellow and purple, respectively, represent that ethane and oxygen are activated inside the heptagonal channel.

in this reaction. The first point is the existence of the micropore where ethane can freely access. The existence of the micropore not only enhance a contact of ethane with activated oxygen, but also weaken the strong C-H bond of ethane due to a possible electric field in the channel. The second point is the α-oxygen defective site which may produce a special oxygen species, like as μ-η^2:η^2-peroxo species as reported to be produced by V dimer in Keggin structure [82-83]. Such molecular level insight for the selective oxidation of ethane could be expressed by the use of the simple but highly multifunctional crystalline oxide catalyst and it can be seen the crucial role of the sophisticated catalyst structure for the selective oxidation. This insight may develop the catalyst design for the selective oxidation of light alkanes.

6. Conclusions

The assembly of the building unit provided from the giant sized and, ball shaped polyoxometalate ($[Mo_{72}V_{30}O_{282}(H_2O)^{56}\cdot(SO_4)_{12}]^{36-}$ ($\{Mo_{72}V_{30}\}$)) produced crystalline Mo_3VO_x oxides with highly organized crystal structure at nano-scale. The comparison of these crystalline catalysts showed that a heptagonal channel in the structure takes part in the catalysis for the selective oxidation of ethane to ethene and of acrolein to acrylic acid. The comparison of the orthorhombic Mo_3VO_x catalysts with tailored crystal sizes unambiguously showed that the heptagonal channel activates ethane inside. On the other hand, acrolein is activated over the channel located on the external surface in the cross-section of the rod-shaped crystal (*a-b* plane). The change in the size of the heptagonal channel strongly affected the catalytic activity for the selective oxidation of ethane. Especially, the evolution of the oxygen which faces to the heptagonal channel increased the number of the active sites for the ethane oxidation which resulted in the enhancement of the catalytic activity.

In this review, we demonstrated the molecular level insight for the catalytic selective oxidations using the structurally well-organized catalyst. Deep understanding of the catalytic reaction may enable us to design the catalytically active site more rationally. We believe that the rational catalyst design based on the understanding of the catalytic reaction at the molecular level finally produces the evolutional catalyst which can achieve dream reactions like as the selective oxidation of methane to methanol or benzene to phenol.

Acknowledgements

This work was supported by JSPS KAKENHI Grant Number 2324-6135.

References

1 A. Chieregato, J. M. L. Nieto and F. Cavani, *Coord. Chem. Rev*., 2014, in press.
2 M. Sun, J. Zhang, P. Putaj, V. Caps, F. Lefebvre, J. Pelletier and J. M. Basset, *Chem. Rev*., 2014, **114**, 981.
3 F. Cavani, *Catal. Today*, 2010, **157**, 8.
4 W. Ueda, K. Oshihara, D. Vitry, T. Hisano and Y. Kayashima, *Catal. Survey Asia*, 2002, **6**, 33.
5 C. Batiot and B. K. Hodnett, *Appl. Catal., A*, 1996, **137**, 179.
6 R. K. Grasselli, *Top. Catal*., 2001, **15**, 93.
7 R. K. Grasselli, *Top. Catal*., 2002, **21**, 79.
8 R. K. Grasselli, *Catal. Today*, 2014, **238**, 10.
9 N. Mizuno and M. Misono, *Chem. Rev.*, 1998**, 98**, 199.
10 G. Koyano, T. Okuhara and M. Misono, *J. Am. Chem. Soc*., 1998, **120**, 767.
11 J. M. Thomas, R. Raja, G. Sankar and R. G. Bell, *Nature*, 1999, **398**, 227.
12 J. M. Thomas, R. Raja, G. Sankar and R. G. Bell, *Acc. Chem. Res*., 2001, **34**, 191.
13 J. M. Thomas and R. Raja, *Proc. Natl. Acad. Sci. USA*, 2005, **102**, 13732.
14 A. B. Getsoian, V. Shapovalov and A. T. Bell, *J. Phys. Chem. C*, 2013, **117**, 7123.
15 A. B. Getsoian, Z. Zhai and A. T. Bell, *J. Am. Chem. Soc*., 2014, **136**, 13684.
16 T. Ushikubo, K. Oshima, A. Kayo, T. Umezawa, K. Kiyono and I. Sawaki, *Eur. Pat.*, 529 852, 1992.
17 T. Ushikubo, K. Oshima, A. Kayo, T. Umezawa, K. Kiyono and I. Sawaki, *US Pat.*, 5 281 745, 1994.
18 T. Ushikubo, H. Nakamura, Y. Koyasu and S. Wagiki, *US Pat.*, 5 380 933, 1995.
19 T. Ushikubo, K. Oshima, A. Kayou, M. Vaarkamp and M. Hatano, *J. Catal*., 1997, **169**, 394.
20 P. Botella, E. G. Gonzalez, A. Dejoz, J. M. L. Nieto, M. I. Vazquez and J. G. Calbet, *J. Catal*., 2004, **225**, 428.
21 T. T. Nguyen, B. Deniau, P. Delichere and J. M. M. Millet, *Top. Catal*., 2014, **57**, 1152.
22 C. Chiu, T. Vogt, L. Zhao, A. Genestc and N. Rösch, *Dalton Trans.*, 2015, **44**, 13778.
23 R. K. Grasselli, D. J. Buttrey, J. D. Burrington, A. Andersson, J. Holmberg, W. Ueda, J. Kubo, C. G. Lugmair and A. F. Volpe, *Top. Catal*., 2006, **38**, 7.
24 Q. He, J. Woo, A. Belianinov, V. V. Guliants and A. Y. Borisevich, *ACS Nano*, 2015, **9**, 3470.
25 P. DeSanto, D. J. Buttrey, R. K. Grasselli, C. G. Lugmair, A. F. Volpe, B. H. Toby and T. Vogt, *Top. Catal*., 2003, **23**, 23.
26 J. M. M. Millet, H. Roussel, A. Pigamo, J. L. Dubois and J. C. Jumas, *Appl. Catal., A*, 2002, **232**, 77.
27 H. Murayama, D. Vitry, W. Ueda, G. Fuchs, M. Anne and J. L. Dubois, *Appl. Catal., A*, 2007, **318**, 137.
28 N. R. Shiju, X. Liang, A. W. Weimer, C. Liang, S. Dai and V. V. Guliants, *J. Am. Chem. Soc*., 2008, **130**, 5850.

29 W. Ueda, N. F. Chen and K. Oshihara, *Chem. Commun*., 1999, 517.
30 W. Ueda and K. Oshima, *Appl. Catal., A,* 2000, **200**, 135.
31 T. Katou, D. Vitry and W Ueda, *Chem. Lett*., 2003, **32**, 1028.
32 T. Katou, D. Vitry and W. Ueda, *Catal. Today*, 2004, **91-92**, 237.
33 H. Watanabe and Y. Koyasu, *Appl. Catal., A*, 2000, **194-195**, 479.
34 R. K. Grasselli, J. D. Burrington, D. J. Buttrey, P. DeSanto, C. G. Lugmair, A. F. Volpe and T. Weingand, *Top. Catal*., 2003, **23**, 5.
35 R. K. Grasselli, *Catal. Today,* 2005, **99**, 23.
36 R. K. Grasselli, C. G. Lugmair and A. F. Volpe, *Top. Catal*., 2008, **50**, 66.
37 W. Ueda, D. Vitry and T. Katou, *Catal. Today*, 2004, **96**, 235.
38 W. Ueda, D. Vitry and T. Katou, *Catal. Today*, 2005, **99**, 43.
39 N. Watanabe and W. Ueda, *Ind. Eng. Chem. Res*., 2006, **45**, 607.
40 W. D. Pyrz, D. A. Blom, N. R. Shiju, V. V. Guliants, T. Vogt and D. J. Buttrey, *J. Phys. Chem. C*, 2008, **112**, 10043.
41 W. D. Pyrz, D. A. Blom, T. Vogt and D. J. Buttrey, *Angew. Chem., Int. Ed.,* 2008, **47**, 2788.
42 X. Li, D. J. Buttrey, D. A. Blom and T. Vogt, *Top. Catal*., 2011, **54**, 614.
43 T. Lunkenbein, F. Girgsdies, A. Wernbacher, J. Noack, G. Auffermann, A. Yasuhara, A. K. Hoffmann, W. Ueda, M. Eichelbaum, A. Trunschke, R. Schlögl and M. G. Willinger, *Angew. Chem., Int. Ed.,* 2015, **54**, 6828.
44 K. Chenoweth, A. C. T. Duin and W. A. Goddard, *Angew. Chem., Int. Ed.*, 2009, **48**, 7630.
45 W. A. Goddard III, J.E. Mueller, K. Chenoweth and A.C.T. Duin, *Catal. Today*, 2010, **157**, 71.
46 L. Zhao, C. C. Chiu, A. Genest and N. Rösch, *Comp. Theor. Chem.*, 2014, **1045**, 57.
47 H. Tsuji and A. Kayou, *J. Am. Chem. Soc*., 2002, **124**, 5608.
48 M. Sadakane, K. Yamagata, K. Kodato, K. Endo, K. Toriumi, Y. Ozawa, T. Ozeki, T. Nagai, Y. Matsui, N. Sakaguchi, W. D. Pyrz, D. J. Buttrey, D. A. Blom, T. Vogt and W. Ueda, *Angew. Chem., Int. Ed.,* 2009, **48**, 3782.
49 R. Canioni, C. M. Roch, N. L. Laronze, M. Haouas, F. Taulèlle, J. Marrot, S. Paul, C. Lamonier, J. F. Paul, S. Loridant, J. M. M. Millet and E. Cadot, *Chem. Commun*., 2011, **47**, 6413.
50 M. S. Sanchez, F. Girgsdies, M. Jastak, P. Kube, R. Schlögl and A. Trunschke, *Angew. Chem., Int. Ed.,* 2012, **51**, 7194.
51 M. Sadakane, K. Endo, K. Kodato, S. Ishikawa, T. Murayama and W. Ueda, *Eur. J. Inorg. Chem*., 2013, **10-11**, 1731.
52 M. Hävecker, S. Wrabetz, J. Kröhnert, L. I. Csepei, R. N. Alnoncourt, Y. V. Kolen'ko, F. Girgsdies, R. Schlögl and A. Trunschke, *J. Catal.* 2012, **285**, 48.
53 R. N. d'Alnoncourt, L. I. Csepei, M. Hävecker, F. Girgsdies, M. E. Schuster, R. Schlögl and A. Trunschke, *J. Catal.*, 2014, **311**, 369.
54 C. Heine, M. Hävecker, M. S. Sanchez, A. Trunschke, R. Schlögl and M. Eichelbaum, *J. Phys. Chem. C*, 2013, **117**, 26988-26997.
55 M. Eichelbaum, M. Hävecker, C. Heine, A. M. Wernbacher, F. Rosowski, A. Trunschke and R. Schlögl, *Angew. Chem., Int. Ed.*, 2015, **54**, 2922.
56 C. Heine, M. Hävecker, A. Trunschke, R. Schlögl and M. Eichelbaum, *Phys. Chem. Chem. Phys.*, 2015, **17**, 8983.
57 G. Mestl , J. L. Margitfalvi, L. Végvári, G. P. Szijjártó and A. Tompos, *Appl. Catal., A*, 2014, **474**, 3.
58 S. H. Morejudo, A. Massó, E. G. González, P. Concepción, and J. M. L. Nieto, *Appl. Catal., A*, in press.
59 S. Ishikawa, X. Yi, T. Murayama and W. Ueda, *Appl. Catal., A*, 2014, **474**, 10.
60 S. Ishikawa, X. Yi, T. Murayama and W. Ueda, *Catal. Today*, 2014, **238**, 35.
61 S. Ishikawa, D. Kobayashi, T. Konya, S. Ohmura, T. Murayama, N. Yasuda, M. Sadakane and W. Ueda, *J. Phys. Chem. C*, 2015, **119**, 7195.
62 M. Sadakane, N. Watanabe, T. Katou, Y. Nodasaka and W. Ueda, *Angew. Chem., Int. Ed.,* 2007, **46**, 1493.
63 T. Konya, T. Katou, T. Murayama, S. Ishikawa, M. Sadakane, D. J. Buttrey and W. Ueda, *Catal. Sci. Technol*., 2013, **3**, 380.
64 M. Sadakane, K. Kodato, T. Kuranishi, Y. Nodasaka, K. Sugawara, N. Sakaguchi, T. Nagai, Y. Matsui and W. Ueda, *Angew. Chem., Int. Ed*., 2008, **47**, 2493.
65 M. Sadakane, S. Ohmura, K. Kodato, T. Fujisawa, K. Kato, K. Shimizu, T. Murayama and W. Ueda, *Chem. Commun*., 2011, **47**, 10812.
66 W. Ueda, *J. Jpn. Petrol. Inst*., 2013, **56**, 122.
67 C. Chen, K. Nakatani, T. Murayama and W. Ueda, *ChemCatChem*., 2013, **5**, 2869.
68 C. Qiu, C. Chen, S. Ishikawa, T. Murayama and W. Ueda, *Top. Catal*., 2014, **57**, 1163.
69 W. Ueda, D. Vitry, T. Katou, N. Watanabe and Y. Endo, *Res. Chem. Intermed*., 2006, **32**, 217.
70 S. Ishikawa, M. Tashiro, T. Murayama and W. Ueda, *Cryst. Growth Des*., 2014, **14**, 4553.
71 K. Itabashi, Y. Kamimura, K. Iyoki, A. Shimojima and T. Okubo, *J. Am. Chem. Soc*., 2012, **134**, 11542.
72 K. Iyoki, K. Itabashi and T. Okubo, *Micropor. Mesopor. Mater*., 2014, **189**, 22.
73 Y. Kamimura, S. Tanahashi, K. Itabashi, A. Sugawara, T. Wakihara, A. Shimojima and T. Okubo, *J. Phys. Chem. C*., 2011, **115**, 744.
74 K. Iyoki, K. Itabashi, W. Chaikittisilp, S. P. Elangovan, T. Wakihara, S. Kohara and T. Okubo, *Chem. Mater*., 2014, **26**, 1957.
75 S. Goel, S. I. Zones and E. Iglesia, *Chem. Mater.*, 2015, **27**, 2056.
76 W. D. Pyrz, D. A. Blom, M. Sadakane, K. Kodato, W. Ueda, T. Vogt and D. J. Buttrey, *Chem. Mater*., 2010, **22**, 2033.
77 W. D. Pyrz, D. A. Blom, M. Sadakane, K. Kodato, W. Ueda, T. Vogt and D. J. Buttrey, *Proc. Natl. Acad. Sci. USA*, 2010, **107**, 6152.
78 C. Liu, S. Zhao, X. Ji, B. Wang and D. Ma, *Mater. Chem. Phys*., 2012, **133**, 579.
79 C. Liu, D. Ma, X. Ji, B. Wang and S. Zhao, *J. Am. Ceram. Soc*., 2011, **94**, 2266.
80 V. P. Valtchev, L. Tosheva and K. N. Bozhilov, *Langmuir*, 2005, **21**, 10724.
81 S. Lee, D. Song, D. Kim, L. Lee, S. Kim, I. Y. Park and Y. D. Choi, *Mater. Lett*., 2004, **58**, 342.
82 K. Kamata, K. Yonehara, Y. Nakagawa, K. Uehara and N. Mizuno, *Nat. Chem*., 2010, **2**, 478.
83 N. Mizuno and K. Kamata, *Coord. Chem. Rev*., 2011, **255**, 2358.

Graphical abstract